Multi-agent Bi-level Game Model for Park-level Integrated Energy System Based on Electricity−Carbon Market Collaborative Decision-making Mechanism

Yumin Zhang, Jingrui Li, Xingquan Ji, Zhaoyang Dong, and Li Yu

Abstract—**Effective coordination between electricity and carbon markets is critical for enabling energy-efficient decarbonization in integrated energy system. However, the inherent differences in trading products and timescales between two markets render independent electricity−carbon market mechanism invalid and target mismatch, particularly within multi-agent market environments. Hence, a multi-agent bi-level game model for park-level integrated energy system (PIES) is proposed in this paper, incorporating a novel electricity−carbon market collaborative decision-making mechanism. An equal-interval time discretization method is developed to reconcile the heterogeneity of discrete electricity market and continuous carbon market, enabling consistent timescale coordination. An improved alternating direction method of multipliers (ADMM) algorithm based on Peaceman-Rachford is adopted to achieve benefit allocation and rapid privacy-solving. Simulation results demonstrate the effectiveness of proposed multi-agent bi-level game model in balancing carbon reduction and economic efficiency, and enhancing the operation efficiency of multi-agent collaboration.**

Index Terms—**Electricity market, carbon market. Decision-making, game model, time discretization, alternating direction method of multipliers (ADMM), multi-agent, integrated energy system (IES).**

I. Introduction

COLLABORATIVE optimization of electricity market and carbon market is essential for achieving energy transition and carbon neutrality goals [1]-[3]. The electricity market is primarily focused on meeting demand through cost-efficient and reliable generation [4], whereas the carbon market seeks to mitigate carbon emissions and facilitate the transition to low carbon energy [5]. Currently, the coordination framework between the electricity market and carbon market involves two main methods. One is linear aggregation of objective functions, while the other adds a fixed carbon price signal to the electricity price [6]-[8]. However, the linear aggregation of objectives fails to capture variations in the mutual influence between the two markets across diverse timescales. And a fixed carbon price signal neglects carbon price volatility, hindering dynamic reflection of market changes on decision-making. Moreover, significant differences in energy resources and demand characteristics among park-level integrated energy systems (PIESs) hinder the existing coordination methods from accommodating inter-park variations and dynamic interactions [9]-[10]. Thus, establishing an electricity−carbon market collaborative decision-making mechanism has become a vital issue for PIESs, with the goal of achieving multi-timescale coordination and multi-agent collaboration.

The electricity market primarily pursues supply-demand equilibrium with an emphasis on economic efficiency [11], realized through short-term behaviors such as competitive bidding and demand response. In [12], a zero-carbon operation framework is developed with dual objectives: maximizing economic gains and minimizing carbon emissions. To implement the goal of environmental friendliness, an optimal scheduling model with low-carbon operation constraints is established in [13]. These studies demonstrate that by participating in electricity market, carbon costs can be transmitted to end users, thereby fully unleashing the potential for carbon emission reduction on the demand side. However, the aforementioned methods fail to fully leverage the carbon price adjustment function, making it challenging to effectively control carbon emissions amid dynamic market fluctuations.

The mechanism in carbon market is generally considered to reflect fluctuations in carbon prices, which plays an important role in influencing market dynamics and supporting the control of carbon emissions [14]. In [15], a ladder-type carbon trading scheme is introduced to incorporate carbon

Manuscript received: May 28, 2025; revised: September 8, 2025; accepted: November 4, 2025. Date of CrossCheck: November 4, 2025. Date of online publication: December 30, 2025.

This work was supported by Shandong Provincial Natural Science Foundation of China (No. ZR2024ME029), Jockey Club Science Technology Engineering and Mathematics Lab of Future Energy Systems (No. 2025-0039), Global Science Technology Engineering and Mathematics Professorship (No. GSP313), and a Startup Grant of City University of Hong Kong, China "Data Driven Real Time Smart Energy Management System Supporting Energy Transition".

Y. Zhang, J. Li, and X. Ji (corresponding author) are all with the Shandong University of Science and Technology, Qingdao 266590, China (e-mail: ymzhang2019@sdust.edu.cn; lijr@sdust.edu.cn; xqji@sdust.edu.cn).

Z. Dong and L. Yu are with the Department of Electrical Engineering, City University of Hong Kong, Hong Kong 999077, China (e-mail: zydong@ieee.org; lynne.yu@synco-global.org).

DOI: 10.35833/MPCE.2025.000463

costs and promote low-carbon operation. In [16], a carbon pricing mechanism based on performance is proposed, aiming to encourage carbon emission reduction through tangible performance outcomes. However, carbon responsibility should be allocated based on actual emissions. Moreover, the aforementioned method fails to reflect the responsibility allocation in terms of emissions and timescale through carbon prices. Accurate calculation of system carbon emission flow (CEF) is essential for precise carbon emission measurement and fair allocation of carbon responsibilities, and it serves as the foundation for the reasonable formulation of carbon prices [17]. The potential mapping relationship of the carbon at the input-output ports of coupled equipment is derived and an integrated electricity-natural gas-heat CEF model is established in [18]. Furthermore, hydrogen energy can be directly and efficiently utilized to achieve zero- or low-carbon emissions. In [19], an electricity-natural gas-hydrogen CEF model for hydrogen production stations is derived, and the contribution to renewable energy accommodation and carbon reduction is validated. However, the absence of detailed modeling for hydrogen production, utilization, and storage processes limits the accuracy of carbon emission calculations during hydrogen system operation.

Through the application of market mechanisms, coordinated operation among interconnected PIES within a regional system can significantly improve economic efficiency and strengthen energy supply adaptability [20]. Distributed optimization methods such as game theory [21], [22], consensus algorithms [23], [24], and the alternating direction method of multipliers (ADMM) algorithm [25], [26] are introduced into multi-agent collaborative market trading. To prevent chaotic competition among agents and mitigate conflicts of interest, allocation strategies based on game theory have garnered extensive attention [27]-[29]. A trading framework for local energy communities is proposed in [30], where cooperative game theory is employed to model the economic behavior of the participants. However, most of these studies overlook the positive impact of various resource couplings on realizing carbon reduction potential. They also fail to explore trading behaviors in electricity market and carbon market across different timescales and trading types.

This paper proposes a multi-agent bi-level game model for PIES based on electricity-carbon market collaborative decision-making mechanism. The main contributions are outlined as follows.

1) To transmit the interaction between electricity market and carbon market, an electricity-carbon market collaborative decision-making mechanism is proposed, considering the coordination of timescales and trading types.

2) An equal-interval time discretization method for the timescale of carbon market is developed, which is compatible with the timescale of the electricity market. An augmented CEF (ACEF) model for PIESs is established, enabling price signal transmission between electricity market and carbon market.

3) An improved ADMM algorithm based on the Peaceman-Rachford (PR) splitting technique is adopted to solve the multi-agent bi-level game model, enabling benefit allocation and rapid privacy-solving.

The rest of this paper is organized as follows. Section II introduces the electricity-carbon market collaborative decision-making mechanism based on ACEF model. Section III describes the multi-agent bi-level game model considering the proposed mechanism. Section IV presents the solution method for the proposed model. Section V analyzes the validation of the proposed mechanism through case studies. Section VI concludes the paper.

II. Electricity-Carbon Market Collaborative Decision-making Mechanism Based on ACEF Model

A. Electricity-Carbon Market Collaborative Decision-making Mechanism

The electricity-carbon market collaborative decision-making mechanism proposed in this paper is aimed at the regional market located at the side of the distribution network. Multi-agents in the region are located at the same transmission network node and obtain free carbon quotas from the government. The market behavior is regulated by the government, with electricity and carbon quotas traded independently within the region. Each agent makes economic and low-carbon decisions by participating in the electricity market and carbon market. The schematic diagram of the proposed mechanism is shown in Fig. 1. Note that the alternating color blocks (green and blue) on the timeline represent different hourly trading periods, corresponding to distinct carbon emission intensities and electricity prices in the day-ahead scheduling horizon.

The electricity-carbon market, based on the relationship between electricity and carbon pricing, regulates unit dispatch, demand-side response, and carbon quota adjustments to achieve a Pareto-efficient outcome. The proposed mechanism mainly includes the following two aspects.

1) Multi-market decision coordination: in traditional markets where electricity and carbon are traded separately, PIESs first participate in the electricity market. They then calculate carbon emissions based on electricity trading and determine whether to enter the carbon market. Such independent electricity-carbon trading markets rely solely on energy information to guide carbon trading, thereby failing to fully exploit the bidirectional incentive mechanisms inherent in the trading process. In the proposed mechanism, PIES simultaneously makes decisions for electricity trading and carbon trading. The bidirectional transmission of electricity and carbon decision results interacts with each other, achieving electricity-carbon market collaborative decision-making behavior.

2) Discretization of carbon market: the collaborative decision-making of PIES in electricity market and carbon market also involves coupling issues between markets at multi-timescales. In the proposed mechanism, the timescale of regional carbon market is discretized to match the timescale of the electricity market.

PIES simultaneously makes decisions in both electricity market and carbon market within a single timescale, achieving collaborative electricity-carbon trading decisions on the same timescale. Additionally, the penalty cost for excess carbon emissions is calculated at the end of the scheduling period. Therefore, changes in carbon allowances resulting from prior trading will influence the decision-making process of the current period, continuously impacting the outcomes. Therefore, the continuity of information for carbon market participants is maintained across different trading periods.

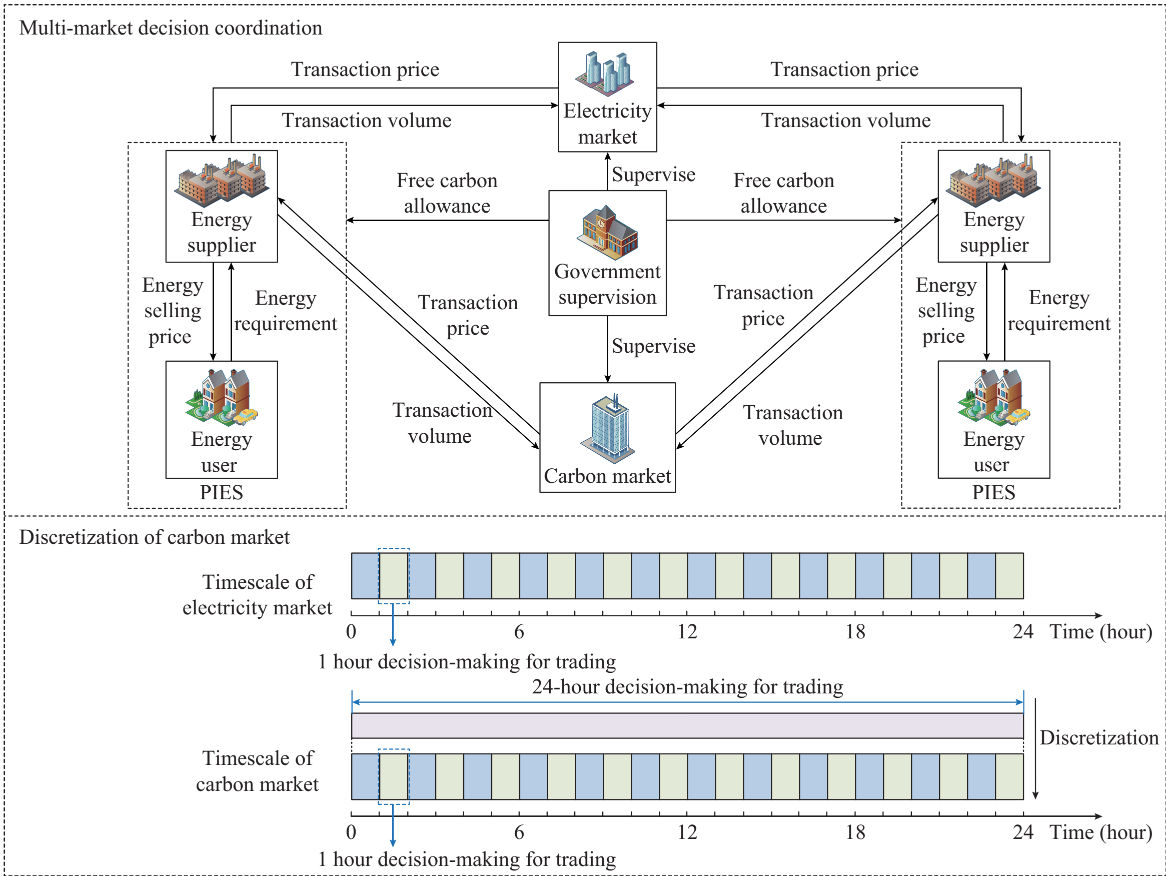

Fig. 1. Schematic diagram of proposed mechanism.

B. Multi-agent Bi-level Game

Under the proposed mechanism, each PIES operates as an independent economic agent, engaging in market-based trading. Through strategic gaming, agents determine electricity and carbon allowance trading volumes to optimize individual revenues. Simultaneously, they reduce overall carbon emissions in accordance with governmental regulation.

Each PIES represents a Stackelberg game issue. At the upper level, the ACEF model is employed to quantify the carbon price at each load node. The external carbon emission cost is reasonably apportioned and internalized as part of the PIES operation cost, thereby generating an electricity−carbon coupling price that is propagated to the lower decision layer. At the lower level, users optimize their energy usage in response to price signals to reduce costs, with the adjusted demand profile subsequently transmitted to the upper level for collaborative decision-making. Then, the scheduling plan of the park can be adjusted at the upper level according to the updated energy consumption demand. Through repeated iterations between the upper and lower levels, the source-load trading equilibrium is achieved.

After each PIES achieves source-load trading equilibrium, multi-PIESs will engage in a cooperative game. Each PIES determines the electricity and carbon allowance trading volumes. To maintain confidentiality between agents, the exchanged information among multi-PIESs is restricted to the electricity and carbon allowance trading volumes. Additionally, only the corresponding trading prices are shared. If there is discrepancy in the market trading, each agent internally adjusts the output plans of each unit, alters energy selling prices, and guides consumers to change their energy consumption behaviors. Decisions are made regarding the optimal trading volume and trading price of each period. The updated information is propagated among agents, and iterative adjustments proceed until a consistent equilibrium is established within and between all agents. The multi-agent bi-level game model consists of an internal source-load Stackelberg game and a multi-agent cooperative game. This model shifts carbon reduction responsibility from the source side to the load side, promoting regional carbon reduction through multi-agent participation in both the electricity market and carbon market.

C. ACEF Model of Green Hydrogen Production

1) Green Hydrogen Production Modeling

The green hydrogen production process primarily consists of three stages: production, storage, and consumption. The involved equipment includes electrolyzer (EL), hydrogen fu-el cell (HFC), methane reactor (MR), and hydrogen storage (HS), with the entire green hydrogen production process shown in Supplementary Material A Fig. SA1.

1) Green hydrogen production process

In EL, renewable energy is employed to electrolyze water to produce hydrogen. The electricity and water consumptions can be expressed as:

$$\begin{cases} V_{\mathrm{EL,H_2},n,t}=\eta_{\mathrm{EL}}\dfrac{P_{\mathrm{EL,e},n,t}}{Q_{\mathrm{H_2}}} \\ M_{\mathrm{H_2O},n,t}=\beta_{\mathrm{H_2O}}V_{\mathrm{EL,H_2},n,t} \\ P_{\mathrm{EL,e}}^{\min}\le P_{\mathrm{EL,e},n,t}\le P_{\mathrm{EL,e}}^{\max} \end{cases} \tag{1}$$

where $V_{\mathrm{EL,H_2},n,t}$ is the green hydrogen output of EL at node n during period t; η_{EL} is the electricity-to-hydrogen conversion efficiency of EL; $P_{\mathrm{EL,e},n,t}$ is the electricity consumption of EL at node n during period t; $Q_{\mathrm{H_2}}$ the lower heating value of hydrogen; $M_{\mathrm{H_2O},n,t}$ is the water consumption of EL at node n during period t; $\beta_{\mathrm{H_2O}}$ is the water consumption coefficient of EL; and $P_{\mathrm{EL,e}}^{\max}$ and $P_{\mathrm{EL,e}}^{\min}$ are the upper and lower limits of the operation power of EL, respectively.

2) Green HS process

The green HS process is similar to that of electricity storage and satisfies:

$$\begin{cases} V_{\mathrm{HS},n,t}=V_{\mathrm{HS},n,t-1}+\eta_{\mathrm{HS}}V_{\mathrm{HS,in},n,t}-\dfrac{V_{\mathrm{HS,out},n,t}}{\eta_{\mathrm{HS}}} \\ V_{\mathrm{HS,min}}\le V_{\mathrm{HS},n,t}\le V_{\mathrm{HS,max}} \\ V_{\mathrm{HS},0}=V_{\mathrm{HS},T} \\ 0\le V_{\mathrm{HS,in},n,t}\le V_{\mathrm{HS,in,max}} \\ 0\le V_{\mathrm{HS,out},n,t}\le V_{\mathrm{HS,out,max}} \end{cases} \tag{2}$$

where $V_{\mathrm{HS},n,t}$ and $V_{\mathrm{HS},n,t-1}$ are the HS capacities at node n during period t and period $t-1$, respectively; $V_{\mathrm{HS,in},n,t}$ and $V_{\mathrm{HS,out},n,t}$ are the amounts of hydrogen input and output of HS at node n during period t, respectively; η_{HS} is the working efficiency of HS; $V_{\mathrm{HS,max}}$ and $V_{\mathrm{HS,min}}$ are the upper and lower limits of HS capacity, respectively; $V_{\mathrm{HS},0}$ and $V_{\mathrm{HS},T}$ are the amounts of hydrogen stored in HS at the beginning and end of the scheduling period, respectively; and $V_{\mathrm{HS,in,max}}$ and $V_{\mathrm{HS,out,max}}$ are the maximum amounts of hydrogen input and output of HS, respectively.

3) Green hydrogen consumption process

HFC can convert green hydrogen produced through electrolysis into both electrical and thermal power, subject to the following constraints:

$$\begin{cases} P_{\mathrm{HFC},n,t}=\eta_{\mathrm{HFC,e}}Q_{\mathrm{H_2}}V_{\mathrm{HFC,H_2},n,t} \\ H_{\mathrm{HFC},n,t}=\eta_{\mathrm{HFC,h}}Q_{\mathrm{H_2}}V_{\mathrm{HFC,H_2},n,t} \\ P_{\mathrm{HFC,min}}\le P_{\mathrm{HFC},n,t}\le P_{\mathrm{HFC,max}} \end{cases} \tag{3}$$

where $P_{\mathrm{HFC},n,t}$ and $H_{\mathrm{HFC},n,t}$ are the electrical and thermal power outputs of HFC at node n during period t, respectively; $\eta_{\mathrm{HFC,e}}$ and $\eta_{\mathrm{HFC,h}}$ are the hydrogen-to-electricity and hydrogen-to-heat conversion efficiencies of HFC, respectively; $V_{\mathrm{HFC,H_2},n,t}$ is the hydrogen consumption of HFC at node n during period t; and $P_{\mathrm{HFC,max}}$ and $P_{\mathrm{HFC,min}}$ are the upper and lower limits of the electrical power outputs of HFC, respectively.

Additionally, the produced green hydrogen is also supplied to MR, where it reacts with carbon dioxide to synthesize methane, which can be expressed as:

$$\begin{cases} V_{\mathrm{MR,CH_4},n,t}=\eta_{\mathrm{MR}}V_{\mathrm{MR,H_2},n,t}\dfrac{Q_{\mathrm{H_2}}}{Q_{\mathrm{CH_4}}} \\ M_{\mathrm{MR,CO_2},n,t}=\beta_{\mathrm{CO_2}}V_{\mathrm{MR,CH_4},n,t} \\ V_{\mathrm{MR,CH_4,min}}\le V_{\mathrm{MR,CH_4},n,t}\le V_{\mathrm{MR,CH_4,max}} \end{cases} \tag{4}$$

where $V_{\mathrm{MR,CH_4},n,t}$ is the volume of natural gas produced by MR at node n during period t; $V_{\mathrm{MR,H_2},n,t}$ is the the volume of hydrogen consumed by MR at node n during period t; η_{MR} is the methanation efficiency of MR; $Q_{\mathrm{CH_4}}$ is the calorific value of natural gas; $M_{\mathrm{MR,CO_2},n,t}$ is the mass of CO_2 consumed by MR at node n during period t; $\beta_{\mathrm{CO_2}}$ is the carbon consumption coefficient of MR; and $V_{\mathrm{MR,CH_4,max}}$ and $V_{\mathrm{MR,CH_4,min}}$ are the upper and lower limits of the volume of natural gas produced by MR, respectively.

2) ACEF Model for Green Hydrogen Production

Based on the CEF model of multi-energy flow system for electricity, natural gas, and heat established in previous work [22], and the CEF models for energy coupling equipment represented by natural gas turbines (GTs) and combined heat and power (CHP) units, the ACEF model for the entire production-consumption-storage process of green hydrogen production can be derived. The CEF for energy coupling equipment adheres to the carbon emission conservation principle, ensuring consistent allocation and transfer of emissions across energy systems.

$$\rho_{\mathrm{in},u,n,t}P_{\mathrm{in},u,n,t}=\rho_{\mathrm{out},u,n,t}P_{\mathrm{out},u,n,t} \tag{5}$$

where $\rho_{\mathrm{in},u,n,t}$ and $\rho_{\mathrm{out},u,n,t}$ are the carbon intensities (CIs) at the input and output ends of equipment u at node n during period t, respectively; and $P_{\mathrm{in},u,n,t}$ and $P_{\mathrm{out},u,n,t}$ are the input and output power of equipment u at node n during period t, respectively.

Regarding EL as a single-input single-output equipment, the relationship between CI at input and output ports of EL can be expressed as:

$$\rho_{\mathrm{in,EL},n,t}P_{\mathrm{EL,e},n,t}=\rho_{\mathrm{out,EL},n,t}V_{\mathrm{EL,H_2},n,t}Q_{\mathrm{H_2}} \tag{6}$$

where $\rho_{\mathrm{in,EL},n,t}$ and $\rho_{\mathrm{out,EL},n,t}$ are the CIs at the input and output ports of EL at node n during period t, respectively. According to (1), $\rho_{\mathrm{out,EL},n,t}$ can be expressed as:

$$\rho_{\mathrm{out,EL},n,t}=\frac{\rho_{\mathrm{in,EL},n,t}}{\eta_{\mathrm{EL}}} \tag{7}$$

Regarding HFC as a single-input multi-output equipment, the relationship between the CI at the input and output ports of HFC can be expressed as:

$$\rho_{\mathrm{in,HFC},n,t}V_{\mathrm{HFC,H_2},n,t}Q_{\mathrm{H_2}}=\rho_{\mathrm{e,HFC},n,t}P_{\mathrm{HFC},n,t}+\rho_{\mathrm{h,HFC},n,t}H_{\mathrm{HFC},n,t} \tag{8}$$

where $\rho_{\mathrm{in,HFC},n,t}$ is the CI at the input port of HFC at node n during period t; and $\rho_{\mathrm{e,HFC},n,t}$ and $\rho_{\mathrm{h,HFC},n,t}$ are the CIs at the electrical and thermal output ports of HFC at node n during period t, respectively. According to (3), we have:

$$\begin{cases} \rho_{\mathrm{e,HFC},n,t} = \dfrac{\rho_{\mathrm{in,HFC},n,t}}{2\eta_{\mathrm{HFC,e}}} \\ \rho_{\mathrm{h,HFC},n,t} = \dfrac{\rho_{\mathrm{in,HFC},n,t}}{2\eta_{\mathrm{HFC,h}}} \end{cases} \tag{9}$$

HS can be considered as an energy storage device, where the carbon emissions associated with the natural gas storage process are quantified as:

$$M_{\mathrm{in,HS},n,t} = \rho_{n,t} V_{\mathrm{HS,in},n,t} Q_{\mathrm{H_2}} \Delta t \tag{10}$$

where $M_{\mathrm{in,HS},n,t}$ is the carbon emission charged into HS at node n during period t; $\rho_{n,t}$ is the CI at node n where HS is located during period t; and Δt is the time interval. During the discharge phase of HS, carbon is released concomitantly with hydrogen as:

$$\rho_{\mathrm{HS},n,t} = \frac{\rho_{\mathrm{HS},n,t-1} V_{\mathrm{HS},n,t-1} + M_{\mathrm{in,HS},n,t} - M_{\mathrm{out,HS},n,t}}{V_{\mathrm{HS},n,t}} \tag{11}$$

$$M_{\mathrm{out,HS},n,t} = \frac{V_{\mathrm{HS,out},n,t} Q_{\mathrm{H_2}}}{\eta_{\mathrm{HS}}} \rho_{\mathrm{HS},n,t-1} \Delta t \tag{12}$$

where $M_{\mathrm{out,HS},n,t}$ is the carbon emission released from HS at node n during period t; and $\rho_{\mathrm{HS},n,t}$ is the CI of HS at node n during period t.

From (4), the amount of CO_2 consumed by MR to produce natural gas during period t is expressed as:

$$M_{\mathrm{MR,CO_2},n,t} = \frac{\beta_{\mathrm{CO_2}} \eta_{\mathrm{MR}} V_{\mathrm{MR,H_2},n,t} Q_{\mathrm{H_2}}}{Q_{\mathrm{CH_4}}} \tag{13}$$

Therefore, the CI at the output port of MR is expressed as:

$$\rho_{\mathrm{MR},n,t} = \frac{M_{\mathrm{MR,CO_2},n,t}}{V_{\mathrm{MR,CH_4},n,t} Q_{\mathrm{CH_4}}} = \frac{\beta_{\mathrm{CO_2}} \eta_{\mathrm{MR}} V_{\mathrm{MR,H_2},n,t} Q_{\mathrm{H_2}}}{V_{\mathrm{MR,CH_4},n,t} Q_{\mathrm{CH_4}}^2} \tag{14}$$

III. Multi-agent Bi-level Game Model Considering Proposed Mechanism

A. Stackelberg Game Optimization Decision Model for PIES

1) Optimization Decision Model of Energy Suppliers

The objective of each PIES is to minimize the operation costs and carbon penalty costs, as expressed in (15)-(20).

$$\min C_i = C_{i,\mathrm{op}} + C_{i,\mathrm{pun}} \tag{15}$$

$$C_{i,\mathrm{op}} = \sum_{t=1}^{T} (C_{i,\mathrm{buy}}(P_{i,t}, G_{i,t}) - C_{i,\mathrm{sell}}(P_{i,t,\mathrm{sell}}) + C_{i,\mathrm{nsp}}(P_{i,t,\mathrm{nsp}} + H_{i,t,\mathrm{nsp}} + G_{i,t,\mathrm{nsp}}) + C_{ij}(p_{ij,t,\mathrm{e}}, q_{ij,t,\mathrm{e}}, p_{ij,t,\mathrm{c}}, q_{ij,t,\mathrm{c}}) + C_{ij,\mathrm{net}}(q_{ij,t,\mathrm{e}}))\Delta t \tag{16}$$

$$C_{i,\mathrm{pun}} = \begin{cases} \delta_{\mathrm{pun}} \left[E_{i,\mathrm{c}} - \left(E_{i,\mathrm{c},0} - \displaystyle\sum_{j \in J, j \neq i} E_{ij,\mathrm{c}} \right) \right] & E_{i,\mathrm{c}} > \left(E_{i,\mathrm{c},0} - \displaystyle\sum_{j \in J, j \neq i} E_{ij,\mathrm{c}} \right) \\ 0 & E_{i,\mathrm{c}} \leq \left(E_{i,\mathrm{c},0} - \displaystyle\sum_{j \in J, j \neq i} E_{ij,\mathrm{c}} \right) \end{cases} \tag{17}$$

$$E_{ij,\mathrm{c}} = \sum_{t=1}^{T} q_{ij,t,\mathrm{c}} \tag{18}$$

$$C_{i,\mathrm{buy}}(P_{i,t}, G_{i,t}) = \delta_{t,\mathrm{buy,e}} P_{i,t} + \delta_{t,\mathrm{buy,g}} G_{i,t} \tag{19}$$

$$C_{i,\mathrm{sell}}(P_{i,t,\mathrm{sell}}) = \delta_{t,\mathrm{sell,e}} P_{i,t,\mathrm{sell}} \tag{20}$$

where J is the set of agents; C_i is the total cost of agent i; $C_{i,\mathrm{op}}$ is the operation cost of agent i including trading cost; $C_{i,\mathrm{pun}}$ is the penalty cost paid by agent i for carbon emissions exceeding the allocated allowance; $C_{i,\mathrm{buy}}(\cdot)$ and $C_{i,\mathrm{sell}}(\cdot)$ are the energy purchasing cost function and energy selling revenue function of agent i, respectively; $C_{i,\mathrm{nsp}}(\cdot)$ is the load shedding penalty cost of agent i; $C_{ij}(\cdot)$ is the trading cost function between agents i and j; $C_{ij,\mathrm{net}}(\cdot)$ is the grid tariff function between agents i and j; $P_{i,t}$ and $G_{i,t}$ are the electricity and natural gas volumes purchased by agent i during period t, respectively; $P_{i,t,\mathrm{sell}}$ is the electricity sold by agent i to the upper-level grid during period t; $P_{i,t,\mathrm{nsp}}$, $H_{i,t,\mathrm{nsp}}$, and $G_{i,t,\mathrm{nsp}}$ are the electricity, heat, and natural gas load shedding volumes of agent i during period t, respectively; $q_{ij,t,\mathrm{e}}$ and $q_{ij,t,\mathrm{c}}$ are the trading volumes of electricity and carbon allowances between agents i and j during period t, respectively; $p_{ij,t,\mathrm{e}}$ and $p_{ij,t,\mathrm{c}}$ are the trading prices of electricity and carbon allowances between agents i and j during period t, respectively; $E_{i,\mathrm{c},0}$ and $E_{i,\mathrm{c}}$ are the free carbon allowance allocated to agent i and the actual carbon emission, respectively; $E_{ij,\mathrm{c}}$ is the total carbon allowance traded between agents i and j; δ_{pun} is the carbon emission excess penalty coefficient; $\delta_{t,\mathrm{buy,e}}$ and $\delta_{t,\mathrm{buy,g}}$ are the electricity and natural gas purchased from the upper-level grid during period t, respectively; and $\delta_{t,\mathrm{sell,e}}$ is the electricity sold by the agent to the upper-level grid during period t. The constraints include the carbon allowance constraints, the constraints of the electricity, natural gas, and heat subsystems, as well as the constraints of coupled devices, as shown in [31].

2) Pricing of Energy Suppliers

The optimal scheduling plan obtained from solving the above model will be used as input to calculate the CI at each load node based on the ACEF model. We adopt the CEF model of electric power system proposed in [17], which is expressed as:

$$\rho_{n,t,\mathrm{NCIe}} = \frac{\displaystyle\sum_{k \in L_{\mathrm{e}}(\cdot,n)} f_{kn,t} \rho_{k,t,\mathrm{NCIe}} + \sum_{g \in G_n} P_{g,t} \rho_{g,t,\mathrm{GCIe}}}{\displaystyle\sum_{l \in L_{\mathrm{e}}(\cdot,n)} f_{kn,t} + \sum_{g \in G_n} P_{g,t}} \tag{21}$$

where G_n is the set of generation units located at node n; $L_{\mathrm{e}}(\cdot,n)$ is the set of electrical lines terminating at node n; $f_{kn,t}$ is the line power flowing from node k to node n during period t; $P_{g,t}$ is the output power of generation unit g during period t; $\rho_{n,t,\mathrm{NCIe}}$ and $\rho_{k,t,\mathrm{NCIe}}$ are the node carbon intensities (NCIs) of nodes n and k during period t, respectively; and $\rho_{g,t,\mathrm{GCIe}}$ is the generation carbon intensity (GCI) of generation unit g during period t.

Similar to the electric power system, the NCI within the natural gas system adheres to the energy distribution principle, which is expressed as:

$$\rho_{n,t,\mathrm{NCIg}} = \frac{\displaystyle\sum_{k \in L_{\mathrm{g}}(\cdot,n)} R_{kn,t,\mathrm{g}} + \sum_{o \in O_n} G_{o,t} \rho_{o,t,\mathrm{GCIg}} B}{\left(\displaystyle\sum_{k \in L_{\mathrm{g}}(\cdot,n)} G_{kn,t} + \sum_{o \in O_n} G_{o,t} \rho_{o,t,\mathrm{GCIg}} \right) B} \tag{22}$$

$$\rho_{o,t,\mathrm{GCIg}} = \frac{E}{B} \tag{23}$$

where $L_{\mathrm{g}}(\cdot,n)$ is the set of natural gas pipelines terminating at node n; O_n is the set of natural gas sources located at node n; $R_{kn,t,\mathrm{g}}$ is the CERF for the natural gas pipeline (k,n) injecting into node n during period t; $G_{o,t}$ is the output power of natural gas source o during period t; $G_{kn,t}$ is the output power of the natural gas pipeline (k,n) injecting into node n during period t; $\rho_{n,t,\mathrm{NCIg}}$ is the NCI of node n during period t; $\rho_{o,t,\mathrm{GCIg}}$ is the GCI of natural gas source o during period t; E is the carbon emission coefficient of natural gas; and B is the calorific value of natural gas, which is set to be 10.45 kWh/m^3, leading to the value of $\rho_{o,t,\mathrm{GCIg}}=0.2$ tCO$_2$/MWh [32].

The heat system comprises heat sources, heat pipelines, and heat loads. The heat generated from the sources is transmitted to the loads via water circulation in the heat pipelines, which are categorized into supply pipelines and return pipelines based on the flow direction of the water. The process of pipeline expansion for the heat system is shown in Supplementary Material A Fig. SA2. Its CEF model is separately computed for the supply and return systems.

$$\rho_{n,t,\mathrm{NCIh,S}}=\frac{\sum\limits_{k\in L_\mathrm{h}(\cdot,n)}\rho_{kn,t,\mathrm{BCIh,S}}c_\mathrm{water}m_{kn,t,\mathrm{S}}(T_{kn,t,\mathrm{SI}}-T_{kn,t,\mathrm{SO}})}{\sum\limits_{k\in L_\mathrm{h}(\cdot,n)}(T_{kn,t,\mathrm{SI}}-T_{kn,t,\mathrm{SO}})m_{kn,t,\mathrm{S}}} \tag{24}$$

$$\rho_{n,t,\mathrm{NCIh,R}}=\frac{\sum\limits_{k\in L_\mathrm{h}(n,\cdot)}\rho_{nk,t,\mathrm{BCIh,R}}c_\mathrm{water}m_{nk,t,\mathrm{R}}(T_{nk,t,\mathrm{RI}}-T_{nk,t,\mathrm{RO}})}{\sum\limits_{k\in L_\mathrm{h}(n,\cdot)}(T_{nk,t,\mathrm{RI}}-T_{nk,t,\mathrm{RO}})m_{nk,t,\mathrm{R}}} \tag{25}$$

where $L_\mathrm{h}(n,\cdot)$ and $L_\mathrm{h}(\cdot,n)$ are the sets of heat pipelines starting and ending at node n, respectively; c_water is the specific heat capacity of the fluid in the heat pipeline network; $m_{kn,t,\mathrm{S}}$ and $m_{nk,t,\mathrm{R}}$ are the heat and return flow rates in the heat pipelines (k,n) and (n,k), respectively; $T_{kn,t,\mathrm{SI}}$ and $T_{kn,t,\mathrm{SO}}$ are the inlet and outlet temperatures of the supply pipeline (k,n) during period t, respectively; $T_{nk,t,\mathrm{RI}}$ and $T_{nk,t,\mathrm{RO}}$ are the inlet and outlet temperatures of the return pipeline (n,k) during period t, respectively; $\rho_{n,t,\mathrm{NCIh,S}}$ and $\rho_{n,t,\mathrm{NCIh,R}}$ are the NCIs for the supply and return nodes during period t, respectively; and $\rho_{kn,t,\mathrm{BCIh,S}}$ and $\rho_{nk,t,\mathrm{BCIh,R}}$ are the branch carbon intensities (BCIs) for the supply and return pipelines during period t, respectively.

The energy selling price during each period is then linked to the CI at each load node through carbon emission cost coefficient. The energy selling price can be expressed as:

$$\zeta_{\omega,d,t}=\zeta_{\omega,d,t,0}+\kappa\rho_{\omega,d,t} \tag{26}$$

where $\zeta_{\omega,d,t}$ is the selling price of energy type ω for load d during period t; $\zeta_{\omega,d,t,0}$ is the initial selling price of energy type ω for load d during period t; κ is the carbon tax; and $\rho_{\omega,d,t}$ is the CI of energy type ω for load d during period t.

3) Optimization Decision Model of Energy Users

In response to upper-level energy price signals, consumers optimize their usage behavior with the objective of minimizing total energy acquisition costs.

$$\min C_{i,\mathrm{user}}=\sum_{t=1}^{T}(\zeta_{i,t,\mathrm{e}}\bar{P}_{i,t}+\zeta_{i,t,\mathrm{g}}\bar{G}_{i,t}+\zeta_{i,t,\mathrm{h}}\bar{H}_{i,t}) \tag{27}$$

where $C_{i,\mathrm{user}}$ is the energy purchasing cost of consumer i; $\zeta_{i,t,\mathrm{e}}$, $\zeta_{i,t,\mathrm{g}}$, and $\zeta_{i,t,\mathrm{h}}$ are the electricity, heat, and natural gas prices of consumer i during period t, respectively; $\bar{P}_{i,t}$, $\bar{G}_{i,t}$, and $\bar{H}_{i,t}$ are the optimized electrical, natural gas, and thermal loads of consumer i during period t, respectively.

The price-based demand response model is employed for both electrical and heat loads. Taking electrical load as an example, the demand response model can be expressed as:

$$\boldsymbol{\Sigma}=\begin{bmatrix}\varepsilon_{xx} & \varepsilon_{xy} & \varepsilon_{xz}\\ \varepsilon_{yx} & \varepsilon_{yy} & \varepsilon_{yz}\\ \varepsilon_{zx} & \varepsilon_{zy} & \varepsilon_{zz}\end{bmatrix} \tag{28}$$

$$\varepsilon_{xx}=\frac{\Delta D_x}{D_x}\left(\frac{\Delta\zeta_x}{\zeta_x}\right)^{-1} \tag{29}$$

$$\varepsilon_{xy}=\frac{\Delta D_x}{D_x}\left(\frac{\Delta\zeta_y}{\zeta_y}\right)^{-1} \tag{30}$$

$$\Delta D_x=\sum_{y=1}^{24}\varepsilon_{xy}\frac{\Delta\zeta_y}{\zeta_y}D_x \tag{31}$$

where ε_{xx}, ε_{yy}, and ε_{zz} are the self-elasticity coefficients of electricity prices during periods x, y, and z, with the remaining coefficients representing cross-elasticities of electricity prices, respectively; ζ_x and $\Delta\zeta_x$ are the original electricity price during period x and the change in electricity price, respectively; ζ_y and $\Delta\zeta_y$ are the original electricity price during period y and the change in electricity price, respectively; and D_x and ΔD_x are the original electrical load during period x and the change in load resulting from price change, respectively.

B. Multi-agent Cooperative Game Model

In multi-agent bi-level game model, we establish a multi-agent cooperative game model based on Nash bargaining theory, which considers both collective and individual rationality in deciding the trading prices and volumes of electricity and carbon allowances. The standard model of Nash bargaining can be expressed as:

$$\begin{cases}\max\prod\limits_{i\in I}(U_i-\bar{U}_i)\\ \text{s.t.}\;\; U_i\geq\bar{U}_i\end{cases} \tag{32}$$

where I is the set of agents participating in the cooperative game; $\bar{U}_i$ is the operation cost of agent i after engaging in the cooperative game; and U_i is the bargaining threat point, corresponding to the operation costs of agent i before engaging in the cooperative game. A nonlinear optimization problem is represented in (32). According to [33], this problem is decomposed into two more tractable subproblems: maximizing cooperative benefits and managing energy trading payments. U_i is derived as:

$$U_i=\min\left(\sum_{t=1}^{T}(C_{i,\mathrm{buy}}(P_{i,t},G_{i,t})-C_{i,\mathrm{sell}}(P_{i,t,\mathrm{sell}})+\right.$$
$$\left.C_{i,\mathrm{nsp}}(P_{i,t,\mathrm{nsp}}+H_{i,t,\mathrm{nsp}}+G_{i,t,\mathrm{nsp}}))\Delta t+C_{i,\mathrm{pun}}\right) \tag{33}$$

1) Subproblem of Maximizing Cooperative Benefits

The augmented Lagrangian function $L_{i,1}(\cdot)$, which represents the subproblem of maximizing the cooperative benefits for agent i, is expressed as:

$$L_{i,1}(\chi_{ij},\chi_{ji},\lambda_{ij,1},\rho_{ij,1})=C_{i,0}+\sum_{j\in J,j\neq i}\lambda_{ij,1}(\chi_{ij}+\chi_{ji})+$$
$$\sum_{j\in J,j\neq i}\frac{\rho_{ij,1}}{2}\left\|\chi_{ij}+\chi_{ji}\right\|_2^2 \tag{34}$$

where $C_{i,0}$ is the total cost of agent i excluding trading costs; χ_{ij} and χ_{ji} are the generalized expressions for electricity and carbon allowance trading volumes between agents i and j, respectively; $\lambda_{ij,1}$ is the Lagrange multiplier for energy coupling constraints between agents i and j; and $\rho_{ij,1}$ is the penalty parameter for the subproblem of maximizing cooperative benefits between agents i and j.

2) Subproblem of Energy Transaction Payment

For agent i, the augmented Lagrangian function $L_{i,2}(\cdot)$ for the subproblem of energy transaction payment can be expressed as:

$$L_{i,2}(\zeta_{ij},\zeta_{ji},\lambda_{ij,2},\rho_{ij,2})=-\ln\left(U_i-C_{i,1}-\sum_{t=1}^{T}C_{ij}(\zeta_{ij},\zeta_{ji})\right)+\sum_{j\in J,j\neq i}\lambda_{ij,2}(\zeta_{ij}-\zeta_{ji})+\sum_{j\in J,j\neq i}\frac{\rho_{ij,2}}{2}\left\|\zeta_{ij}-\zeta_{ji}\right\|_2^2 \tag{35}$$

where $C_{i,1}$ is the optimal solution of subproblem of maximizing cooperative benefits; ζ_{ij} and ζ_{ji} are the generalized expressions for the trading prices of electricity and carbon allowances between agents i and j, respectively; $\lambda_{ij,2}$ is the Lagrange multiplier for the subproblem of energy trading payment; and $\rho_{ij,2}$ is the penalty parameter for the subproblem of energy trading payment.

IV. Solution Method for Proposed Model

A. Solution Based on PR-ADMM Algorithm

The PR-ADMM algorithm is based on the concept of PR splitting and involves introducing an intermediate Lagrange multiplier $\lambda_{ij,k+1/2}$ on the basis of the traditional ADMM algorithm [34], essentially performing two iterations on the Lagrange multiplier λ. When the information is transmitted between agents i and j in the forward direction $i\rightarrow j$, a half power multiplier penalty term is added on the basis of the original dual variable. This term is used for the iterative update during the reverse information transmission. Conversely, during the reverse direction $i\leftarrow j$, another penalty term is added to $\lambda_{ij,k+1/2}$ and used for the next iteration update to speed up convergence. Simultaneously, the penalty parameter ρ is multiplied by a relaxation factor $\alpha\in(0,1)$ to ensure that the iteration is strictly converged. The convergence of the aforementioned iterative method is strictly proven in [35].

$$\begin{cases}\chi_{ij,k+1}=\arg\min\limits_{\chi_{ij}} L_i(\chi_{ij,k},\chi_{ji,k},\lambda_{ij,k},\rho_{ij,k})\\ \lambda_{ij,k+1/2}=\lambda_{ij,k}+\alpha\rho_{ij,k}(\chi_{ij,k+1}+\chi_{ji,k})\\ \chi_{ji,k+1}=\arg\min\limits_{\chi_{ji}} L_j(\chi_{ij,k+1},\chi_{ji,k},\lambda_{ij,k+1/2},\rho_{ij,k})\\ \lambda_{ij,k+1}=\lambda_{ij,k+1/2}+\alpha\rho_{ij,k}(\chi_{ij,k+1}+\chi_{ji,k+1})\end{cases} \tag{36}$$

where k is the iteration of the PR-ADMM algorithm; $\chi_{ij,k}$ and $\chi_{ji,k}$ are the generalized expressions for the electricity and carbon trading allowances between agents i and j in the k^{th} iteration, respectively; $\chi_{ij,k+1}$ and $\chi_{ji,k+1}$ are the generalized expressions for the electricity and carbon trading allowances between agents i and j in the $(k+1)^{\text{th}}$ iteration, respectively; $\lambda_{ij,k}$ is the Lagrange multiplier for the energy coupling constraint between agents i and j in the k^{th} iteration; and $\rho_{ij,k}$ is the penalty coefficient for the subproblem of maximizing cooperative benefits between agents i and j in the k^{th} iteration.

The convergence in the PR-ADMM algorithm is determined by verifying whether the primal and dual residuals fall within the predefined tolerance levels.

$$\begin{cases}|r_{ij,k+1}|=|\chi_{ij,k+1}+\chi_{ji,k+1}|\leq\varepsilon_{\text{pri}}\\ |s_{ij,k+1}|=|\rho_{ij,k+1}(\chi_{ij,k+1}+\chi_{ji,k+1})|\leq\varepsilon_{\text{dual}}\end{cases} \tag{37}$$

where $r_{ij,k+1}$ and $s_{ij,k+1}$ are the primal and dual residuals between agents i and j in the $(k+1)^{\text{th}}$ iteration, respectively; $\rho_{ij,k+1}$ is the penalty coefficient for the subproblem of maximizing cooperative benefits between agents i and j in the $(k+1)^{\text{th}}$ iteration; and ε_{pri} and $\varepsilon_{\text{dual}}$ are the convergence tolerances for the primal and dual residuals, respectively.

In PIES, the optimization decision model of Stackelberg game is solved using the alternating iteration method. The convergence criterion is that the variation in prices of various types of energy on the supply side is less than or equal to the given convergence tolerance.

$$|\zeta_{\omega,i,t,\tau}-\zeta_{\omega,i,t,\tau-1}|\leq\varepsilon_{\text{price}} \tag{38}$$

where $\varepsilon_{\text{price}}$ is the convergence tolerance for the optimization decision model of Stackelberg game; and $\zeta_{\omega,i,t,\tau}$ and $\zeta_{\omega,i,t,\tau-1}$ are the selling prices of energy type ω for consumer i during period t in the τ^{th} and $(\tau-1)^{\text{th}}$ iterations, respectively.

B. Solution Process of PR-ADMM Algorithm

The solution process of PR-ADMM algorithm is shown in Algorithm 1, where k_1 and k_2 are the iteration number counters.

Algorithm 1: PR-ADMM algorithm

1. **Input**: ε_{pri}, $\varepsilon_{\text{dual}}$, and $\varepsilon_{\text{price}}$
2. **Initialize**: $k_1\leftarrow 1$. Set values for $\lambda_{ij,1}$ and $\rho_{ij,1}$
3. **Repeat**:
    1) $\tau\leftarrow 1$. Initialize values for $P_{i,t}$, $G_{i,t}$, $H_{i,t}$, $\zeta_{\omega,d,t,0}$, and κ
    2) **Repeat**:
    3) Solve (15) to obtain χ_{ij} and χ_{ji}; and solve ACEF model to obtain $\rho_{\omega,d,t}$
    4) Let $\zeta_{\omega,d,t}\leftarrow\zeta_{\omega,d,t,0}+\kappa\rho_{\omega,d,t}$
    5) Solve (22) to retrieve $P_{i,t}$, $G_{i,t}$, and $H_{i,t}$
    6) Let $\tau\leftarrow\tau+1$
    7) **Until** $|\zeta_{\omega,i,t,\tau}-\zeta_{\omega,i,t,\tau-1}|\leq\varepsilon_{\text{price}}$
4. Let $|r_{ij,k_1+1}|\leftarrow|\chi_{ij,k_1+1}+\chi_{ji,k_1+1}|$ and $|s_{ij,k_1+1}|\leftarrow|\rho_{ij,k_1+1}(\chi_{ij,k_1+1}+\chi_{ji,k_1+1})|^2$
5. $\lambda_{ij,1}$, $\rho_{ij,1}\leftarrow$ (36), (39)
6. $k_1\leftarrow k_1+1$
7. **Until** $|r_{ij,k_1+1}|\leq\varepsilon_{\text{pri}}$ and $|s_{ij,k_1+1}|\leq\varepsilon_{\text{dual}}$
8. **Input**: χ_{ij} and χ_{ji}
9. **Initialize**: $k_2\leftarrow 1$. Set values for $\lambda_{ij,2}$ and $\rho_{ij,2}$
10. **Repeat**:
11. Solve (15) to obtain ζ_{ij} and ζ_{ji}
12. Let $|r_{ij,k_2+1}|\leftarrow|\zeta_{ij,k_2+1}+\zeta_{ji,k_2+1}|$ and $|s_{ij,k_2+1}|\leftarrow|\rho_{ij,k_2+1}(\zeta_{ij,k_2+1}+\zeta_{ji,k_2+1})|^2$
13. $\lambda_{ij,2}$, $\rho_{ij,2}\leftarrow$ (36), (39)
14. $k_2\leftarrow k_2+1$
15. **Until** $|r_{ij,k_2+1}|\leq\varepsilon_{\text{pri}}$ and $|s_{ij,k_2+1}|\leq\varepsilon_{\text{dual}}$

C. Update of Penalty Parameter

The setting of the penalty parameter is crucial for the convergence and stability of the algorithm. A too large penalty parameter may lead to overfitting, causing the optimal solution to be unstable, while a too small penalty parameter that may fail to effectively constrain the optimization model, resulting in an inaccurate solution. The initial value of the penalty parameter is often preset based on empirical values. This paper proposes a strategy to dynamically update the penalty parameter based on the PR-ADMM algorithm, selecting different $\rho_{ij,k}$ according to primal and dual residuals.

$$\rho_{ij,k+1}=\begin{cases}\phi_{\text{in}}\rho_{ij,k} & |r_{ij,k}|>\varphi|s_{ij,k}| \\ \dfrac{\rho_{ij,k}}{\phi_{\text{de}}} & |r_{ij,k}|<\varphi|s_{ij,k}| \\ \rho_{ij,k} & \text{else}\end{cases} \tag{39}$$

where ϕ_{in} and ϕ_{de} are the increase and decrease factors, respectively; $r_{ij,k}$ and $s_{ij,k}$ are the primal and dual residuals between agents i and j in the k^{th} iteration, respectively; and φ is the proportional coefficient.

According to (39), the penalty parameter is dynamically adjusted based on the size of the error. When the constraint error is large, the penalty parameter can be increased to more tightly enforce the constraint. When the constraint error is small, the penalty parameter is reduced, allowing the algorithm more freedom to search for a better solution and accelerating the convergence to the optimal solution. Thus, the initial values are set to be $\lambda=0$ and $\rho=0.1$.

V. Case Study

In order to validate the effectiveness of the proposed mechanism and PR-ADMM algorithm, three representative PIESs with different resource endowments are selected. Among them, PIES1 and PIES2 represent intensive areas of energy consumption, equipped with distributed wind power and distributed photovoltaics (PVs), respectively. PIES3 represents a low energy consumption area with abundant renewable energy, equipped with distributed wind power, distributed PVs, and green hydrogen production equipment. A small-scale system and a relatively large-scale system are used to validated the proposed mechanism. The former consists of an E9-G6-H6 system, which includes a 9-node power grid, a 6-node natural gas network, and a 6-node heat network, as well as an E9-G6-H6 system and an E7-G6-H6 system. The latter consists of an E85-G30-H30 system, an E69-G18-H18 system, and an E33-G10-H6 system. Detailed system parameters are referred to [36] and [37]. The penalty coefficient for exceeding the free carbon allowance is 0.06 \$/kgCO_2e, and the carbon emission cost coefficient is set to be 0.02 \$/kgCO_2e [38]. Note that CO_2e represents the carbon dioxide equivalent. The electricity purchased from the upper-level grid is set according to the time-of-use price. The model is solved by MATLAB software coupled with the Gurobi solver, running on a Windows 11 system powered by an Intel Core i7-13700H CPU at 2.4 GHz and 32 GB of RAM. The scheduling cycle covers 24 hours with one-hour intervals.

Three cases are designed to compare and validate the proposed mechanism. Additionally, the impact of green hydrogen production equipment on reducing operation costs and carbon emissions is evaluated.

1) Case 1: multi-PIESs engage in negotiations in separate electricity market and carbon market, with no information exchange or price coordination between them, and PIES3 operates without green hydrogen production equipment.

2) Case 2: multi-PIESs engage in negotiations under the proposed mechanism, and PIES3 operates without green hydrogen production equipment.

3) Case 3: multi-PIESs engage in negotiations under the proposed mechanism, and PIES3 operates with green hydrogen production equipment.

A. Effectiveness Analysis of Proposed Mechanism

The performance of the proposed mechanism is evaluated by comparing the operation costs and carbon emissions of each PIES and the overall system across Case 1 and Case 2, with detailed results summarized in Table I.

TABLE I
OPERATION RESULTS OF PIESs IN THREE CASES

Case	PIES	Operation cost (\$)	Actual carbon emission (t)	Traded carbon allowance (t)	Accounted carbon emission (t)
Case 1	PIES1	7125.24	14.91	1.15	13.76
	PIES2	6968.25	14.49	0.95	13.54
	PIES3	6280.92	10.80	–2.10	12.90
	Total	20374.41	40.20		40.20
Case 2	PIES1	6984.58	14.86	1.16	13.70
	PIES2	6886.07	14.47	0.97	13.50
	PIES3	6225.53	10.77	–2.13	12.90
	Total	20096.18	40.10		40.10
Case 3	PIES1	6974.70	14.85	1.16	13.69
	PIES2	6842.64	14.45	0.99	13.46
	PIES3	6093.27	10.74	–2.15	12.89
	Total	19910.61	40.04		40.04

From Table I, it is evident that the proposed mechanism reduces the total operation costs of the PIES. Specifically, it achieves a 1.37% reduction compared with the independent electricity−carbon market mechanism. In Case 1, PIESs participate in the electricity market to procure electricity for meeting their load demand. They also separately engage in the carbon market to purchase allowances, covering any excess emissions at the end of the scheduling horizon. Decisions are made unilaterally, and agents continue purchasing electricity even when trading prices are relatively high, thereby failing to achieve economic optimization. In Case 2, the proposed mechanism is employed, which fully considers the price signals within the same time period. During the negotiation process, agents can simultaneously decide on energy trading or carbon allowance trading. Thus, the proposed mechanism demonstrates momentous advantages in both economic efficiency and carbon reduction.

B. Effectiveness Analysis of Green Hydrogen Production

To verify the effectiveness of green hydrogen production equipment for PIES3 and the entire region in both economic efficiency and carbon reduction, we compare the operation results of Case 2 and Case 3, as shown in Table I. Compared with Case 2, the actual carbon emissions of PIES3 in Case 3 decrease by 0.23%. Additionally, the operation costs of PIES3 and total operation costs decrease by 2.12% and 0.92%, respectively. The underlying reason is that PIES3, endowed with abundant renewable resources, can utilize green hydrogen production technologies to supply zero-carbon hydrogen. The green hydrogen output can further serve as a clean energy carrier for the production of zero-carbon electricity and heat. When used in methanation, it can consume a certain amount of carbon dioxide, effectively reducing the carbon emissions of PIES3. Additionally, as a member of the regional cooperative alliance, PIES3 seeks to reduce the trading price of electricity produced from green hydrogen, which contributes to a reduction in the total operation costs.

C. Trading Result Under Proposed Mechanism

To validate the effect of the proposed mechanism on trading results through the interaction of electricity and carbon information during different periods, the electricity trading volume and trading price in Case 2 are compared with those in Case 1. The results are shown in Supplementary Material A Fig. SA3 and Fig. SA4. Compared with the independent electricity‑carbon market mechanism, the outcomes under the proposed mechanism are influenced by the carbon allowance trading volume. Consequently, trading volumes are reduced during the majority of periods.

Combined with the electricity trading price shown in Supplementary Material A Fig. SA4(a) and Fig. SA4(b), in Case 1, during 01:00-05:00, 14:00, and 23:00-04:00, the electricity trading price is close to the grid electricity price. The reason why PIES still chooses to trade electricity is that the carbon emission penalty costs are borne by the seller. Since the trading price is below the grid electricity price that includes carbon penalties, the PIES achieves lower operation costs relative to direct grid procurement. In Case 2, the electricity trading volume during the aforementioned periods decreases. The underlying reason is that a trading price close to the grid electricity price enables the PIES to react efficiently within the carbon market, leveraging the price signals from the electricity market. Agents can purchase the remaining carbon allowances from other PIES in advance, thereby reducing electricity trading volume. This allows for trading decisions that balance both low carbon emissions and economic efficiency. As a result, the operation costs in energy-intensive core areas are significantly reduced.

In summary, the proposed mechanism demonstrates economic and low-carbon advantages in the optimized operation among PIESs. It also highlights the impact of energy-carbon information interaction on trading volume and price over different periods. Furthermore, due to differences in load demand and renewable energy configurations across PIES, each agent exhibits distinct resource trading tendencies. These tendencies evolve throughout the scheduling period, guided by the proposed mechanism. This indicates that the complementary resource advantages and the cooperative game among the parks are crucial for optimizing regional resource allocation. Consequently, this cooperation contributes to the realization of low-carbon economic scheduling.

D. Effectiveness of ACEF Model

In order to demonstrate the validity of the proposed ACEF model, two typical scheduling periods are examined to analyze the CEF behavior of PIES3. Figure 2 shows the ACEF of PIES3 at 02: 00, where the red and blue pipelines and loads represent the supply and return systems of the heat system, respectively. Supplementary Material A Fig. SA5 shows the corresponding CEF pathways from energy sources to consumers.

1) Period 1: 02: 00, which represents the valley of load and the peak of renewable energy output.

2) Period 2: 13:00, which represents the peak of load and the valley of renewable energy output.

From Fig. 2, it can be observed that during period 1, MR uses hydrogen to synthesize methane for CHP, consuming 39.64 kg of CO_2. This is because, during this period, the output of renewable energy generation exceeds the electric load demand, allowing excess energy to be used by EL to produce green hydrogen. This green hydrogen is further combined with CO_2 in MR to generate methane that can be consumed by CHP. On one hand, CI at the terminal of CHP is reduced, which is beneficial to the reduction of carbon emissions of the entire system. On the other hand, it reduces the amount of natural gas purchased from natural gas sources, which reduces the energy supply costs of the system. From Supplementary Material A Fig. SA5, it can be observed that there is no excess renewable energy available for green hydrogen production during period 2, and the equivalent for green hydrogen production equipment is inactive. Green hydrogen technology enhances renewable energy utilization, thereby reducing system supply costs and carbon emissions. The results during period 1 reveal that the total carbon emissions at the supply end of PIES3 are 242.41 kg, while the total carbon emissions at the output end are 172.33 kg. The amounts of carbon emission from losses of the compressor and the heat system are 30.44 kg, MR consumes 39.64 kg, and the total carbon emissions achieve a balance.

During this period, the system exhibits a relatively low level of carbon emissions, mainly due to the reverse peak-shaving characteristic of wind power. The wind power is prioritized to meet the load demand, resulting in a lower CI. In contrast, during period 2, the total carbon emissions at the supply end are 445.21 kg, while the total carbon emissions at the output end are 391.91 kg. The carbon emission from losses of the compressor and the heat system is 53.3 kg, maintaining the conservation of total carbon emissions within the system. There is no excess green electricity available for green hydrogen production during period 2, necessitating the purchase of more natural gas to meet the load demand. This results in a higher overall CI of PIES3 during period 2.

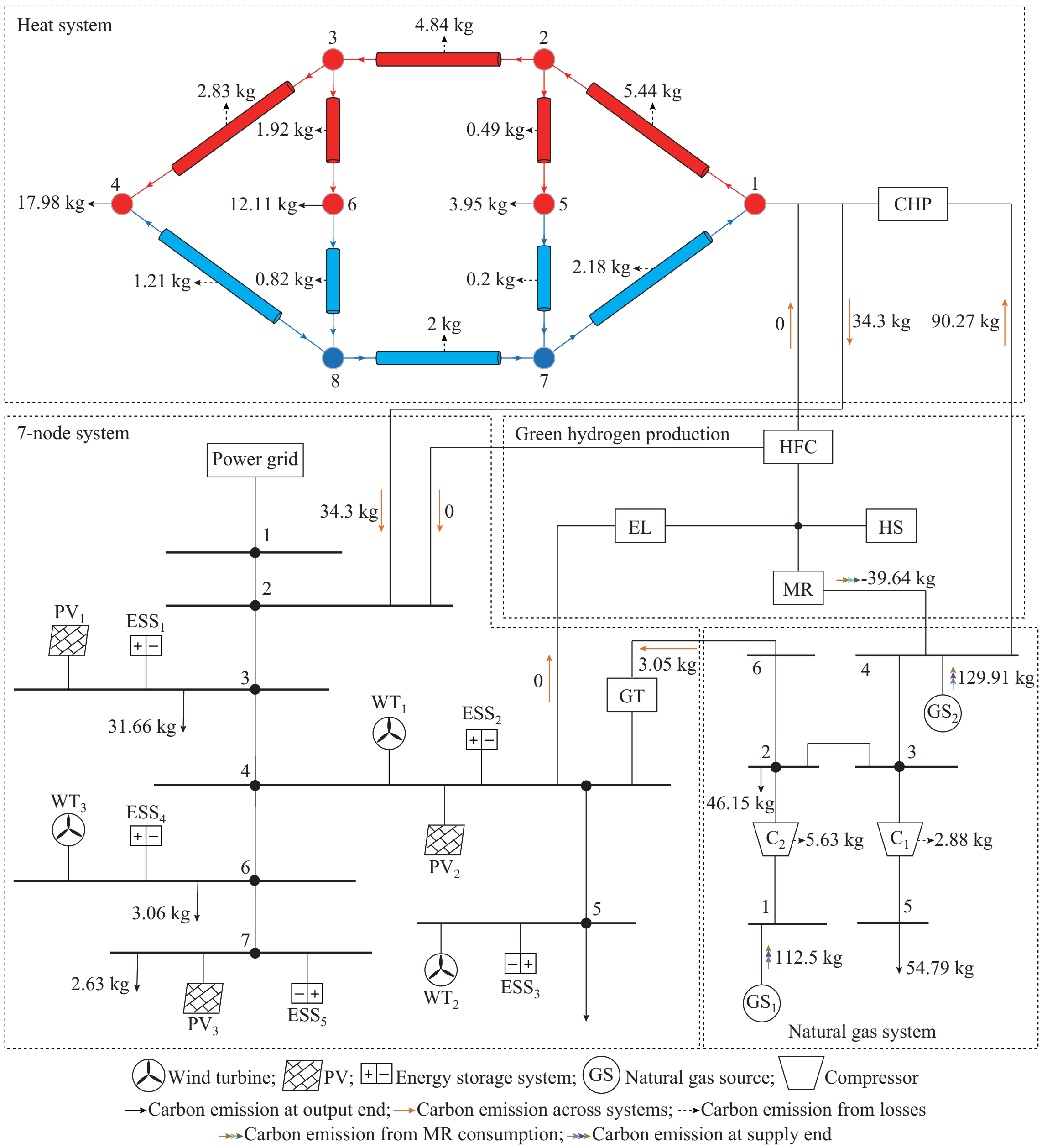

Fig. 2. ACEF of PIES3 at 02:00.

E. Effectiveness Analysis of PR-ADMM Algorithm

To analyze the sensitivity of the PR-ADMM algorithm with different convergence accuracies, Supplementary Material A Table SAI presents the computational results of the PR-ADMM algorithm under different convergence accuracies. As the convergence accuracy increases, the total cost of the PR-ADMM algorithm gradually decreases. Meanwhile, the number of iterations and the computational costs also increase with higher accuracy. However, when the accuracy is set to be 10^{-5}, the total cost decreases slightly, while the iteration time increases significantly. Therefore, a convergence accuracy of 10^{-4} is selected in this paper.

A comparative analysis with the widely used traditional ADMM algorithm is conducted to validate the superior solution efficiency of the PR-ADMM algorithm. The analysis focuses on solving the cooperative benefit maximization subproblem in Case 3. The comparison of calculation efficiency of different algorithms is shown in Table II. And the residual convergence curve of the PR-ADMM algorithm is shown in Fig. 3.

TABLE II
COMPARISON OF CALCULATION EFFICIENCY OF DIFFERENT ALGORITHMS

Algorithm	Total operation cost ($)	Solution time (s)	Number of iterations
Traditional ADMM	209342.56	2573.78	19
PR-ADMM	207660.51	1843.08	13

From Table II, it is evident that compared with traditional ADMM algorithm, the total operation cost of the PR-ADMM algorithm is reduced by 0.81%, the solution time is reduced by 28.39%, and the number of iterations is reduced by 31.58%, demonstrating significant advantage in computational efficiency. In combination with Fig. 3, it can be observed that the PR-ADMM algorithm achieves convergence within only 13 iterations, which has obvious advantages in both solution efficiency and accuracy. This improvement is attributed to the half-step update of the Lagrange multipliers in each iteration of the PR-ADMM algorithm, effectively enhancing the convergence performance.

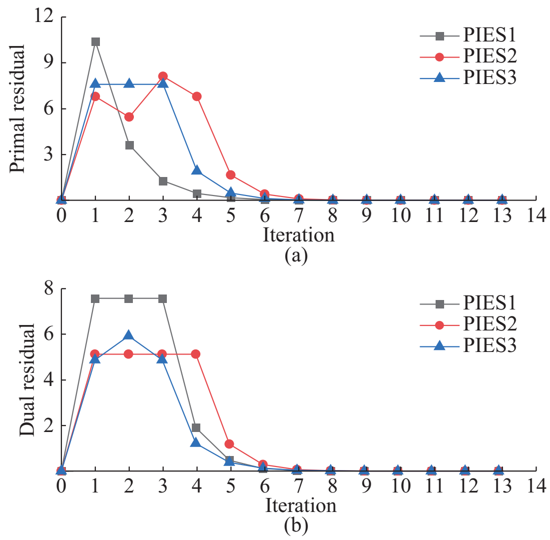

Fig. 3. Residual convergence curve of PR-ADMM algorithm. (a) Primal residual convergence curve. (b) Dual residual convergence curve.

VI. Conclusion

This paper proposes an electricity−carbon market collaborative decision-making mechanism for market participants. The main conclusions are as follows.

1) The proposed mechanism realizes the coordination of strategies in multiple markets on the same timescale. Compared with independent electricity−carbon market mechanism, the total operation cost of the PIESs has been reduced by 1.37%.

2) The established ACEF model can achieve a tight coupling of energy flow and carbon flow. By utilizing node-level carbon intensity indicators, carbon signals are transferred from the supply side to the demand side, fostering user engagement in patterns of low-carbon energy usage.

3) The PR-ADMM algorithm increases the update frequency of dual variables in the process of solving the multi-agent bi-level game model. The solution time is reduced by 28.39% and the number of iterations is reduced by 31.58%.

In future work, the research will explore the integration of the carbon market and electricity market over extended time horizons, with a focus on developing joint decision-making mechanisms under multi-period conditions.

References

[1] P. Härtel and M. Korpås, "Demystifying market clearing and price setting effects in low-carbon energy systems," *Energy Economics*, vol. 93, p. 105051, Jan. 2021.

[2] K. Jiang, N. Liu, X. Yan et al., "Modeling strategic behaviors for Genco with joint consideration on electricity and carbon markets," *IEEE Transactions on Power Systems*, vol. 38, no. 5, pp. 4724-4738, Sept. 2023.

[3] K. Jiang, K. Wang, L. Yang *et al.*, "Reinforcement learning- and option-jointed modeling for cross-market and cross-time trading of generators in electricity and carbon markets," *Journal of Modern Power Systems and Clean Energy*, vol. 13, no. 2, pp. 637-649, Mar. 2025.

[4] L. Wang, C. Dou, D. Yue *et al.*, "Energy sharing market with dual time scale coordination considering new energy uncertainties and competition among stakeholders," *IEEE Transactions on Energy Markets, Policy and Regulation*, vol. 3, no. 3, pp. 309-323, Sept. 2025.

[5] Z. Lu, L. Yan, J. Wang *et al.*, "A market-clearing-based sensitivity model for locational marginal and average carbon emission," *IEEE Transactions on Energy Markets, Policy and Regulation*, vol. 2, no. 4, pp. 579-582, Dec. 2024.

[6] J. Dulipala and S. Debbarma, "Energy scheduling model considering penalty mechanism in transactive energy markets: a hybrid approach," *International Journal of Electrical Power & Energy Systems*, vol. 129, no. 3, p. 106742, Jul. 2021.

[7] Y. Xiang, M. Fang, J. Liu *et al.*, "Distributed dispatch of multiple energy systems considering carbon trading," *CSEE Journal of Power and Energy Systems*, vol. 9, no. 2, pp. 459-469, Mar. 2023.

[8] L. Wang, Y. Zhang, W. Song *et al.*, "Stochastic cooperative bidding strategy for multiple microgrids with peer-to-peer energy trading," *IEEE Transactions on Industrial Informatics*, vol. 18, no. 3, pp. 1447-1457, Mar. 2021.

[9] Z. Zhang, Y. Wang, C. Wang *et al.*, "Distributed chance-constrained optimal dispatch for integrated energy system with electro-thermal couple and wind-storage coordination," *IEEE Transactions on Industry Applications*, vol. 61, no. 1, pp. 833-846, Jan. 2025.

[10] X. Xue, J. Fang, X. Ai *et al.*, "A fully distributed ADP algorithm for real-time economic dispatch of microgrid," *IEEE Transactions on Smart Grid*, vol. 15, no. 1, pp. 513-528, Jan. 2024.

[11] P. You, Y. Jiang, E. Yeung *et al.*, "On the stability, economic efficiency, and incentive compatibility of electricity market dynamics," *IEEE Transactions on Automatic Control*, vol. 70, no. 10, pp. 6815-6830, Oct. 2025.

[12] L. Ju, Z. Yin, Q. Zhou *et al.*, "Nearly-zero carbon optimal operation model and benefit allocation strategy for a novel virtual power plant using carbon capture, power-to-gas, and waste incineration power in rural areas," *Applied Energy*, vol. 310, p. 118618, Mar. 2022.

[13] J. Shen, M. Li, Z. Lin *et al.*, "Low-carbon operation constrained two-stage stochastic energy and reserve scheduling: a worst-case conditional value-at-risk approach," *Electric Power Systems Research*, vol. 225, p. 109833, Dec. 2023.

[14] L. Wang, R. Xian, P. Jiao *et al.*, "Multi-timescale optimization of integrated energy system with diversified utilization of hydrogen energy under the coupling of green certificate and carbon trading," *Renewable Energy*, vol. 228, p. 120597, Jul. 2024.

[15] R. Wang, X. Wen, X. Wang *et al.*, "Low carbon optimal operation of integrated energy system based on carbon capture technology, LCA carbon emissions and ladder-type carbon trading," *Applied Energy*, vol. 311, p. 118664, Apr. 2022.

[16] N. Yan, G. Ma, X. Li *et al.*, "Low-carbon economic dispatch method for integrated energy system considering seasonal carbon flow dynamic balance," *IEEE Transactions on Sustainable Energy*, vol. 14, no. 1, pp. 576-586, Jan. 2023.

[17] Y. Cheng, N. Zhang, Y. Wang *et al.*, "Modelling carbon emission flow in multiple energy system," *IEEE Transactions on Smart Grid*, vol. 10, pp. 3562-3574, Apr. 2019.

[18] Y. Zhang, P. Sun, X. Ji *et al.*, "Low-carbon economic dispatch of integrated energy systems considering full-process carbon emission tracking and low carbon demand response," *IEEE Transactions on Network Science and Engineering*, vol. 11, no. 6, pp. 5417-5437, Dec. 2024.

[19] X. Wei, X. Zhang, Y. Sun *et al.*, "Carbon emission flow-oriented tri-level planning of integrated electricity-hydrogen-gas system with hydrogen vehicles," *IEEE Transactions on Industry Applications*, vol. 58, no. 2, pp. 2607-2618, Mar. 2022.

[20] W. Lyu, Z. Cui, M. Yuan *et al.*, "Cooperation for trans-regional electricity trading from the perspective of carbon quota: a cooperative game approach," *International Journal of Electrical Power & Energy Systems*, vol. 156, p. 109773, Feb. 2023.

[21] W. Zhong, S. Xie, K. Xie *et al.*, "Cooperative P2P energy trading in active distribution networks: a MILP-based Nash bargaining solution," *IEEE Transactions on Smart Grid*, vol. 12, no. 2, pp. 1264-1276, Mar. 2021.

[22] C. Li, Z. Yan, Y. Yao *et al.*, "Coordinated low-carbon dispatching on source-demand side for integrated electricity-gas system based on inte-

grated demand response exchange," *IEEE Transactions on Power Systems*, vol. 39, no. 1, pp. 1287-1303, Jan. 2024.

[23] A. Eladl, M. El-Afifi, M. El-Saadawi *et al*., "Distributed optimal dispatch of smart multi-agent energy hubs based on consensus algorithm considering lossy communication network and uncertainty," *CSEE Journal of Power and Energy Systems*, vol. 11, no. 1, pp. 352-364, Jan. 2023.

[24] B. Alhasnawi, B. Jasim, and B. Sedhom, "Distributed secondary consensus fault tolerant control method for voltage and frequency restoration and power sharing control in multi-agent microgrid," *International Journal of Electrical Power & Energy Systems*, vol. 133, p. 107251, Dec. 2021.

[25] A. Rajaei, S. Fattaheian-Dehkordi, M. Fotuhi-Firuzabad *et al*., "Decentralized transactive energy management of multi-microgrid distribution systems based on ADMM," *International Journal of Electrical Power & Energy Systems*, vol. 132, p. 107126, Nov. 2021.

[26] Y. He, Q. Chen, J. Yang *et al*., "A multi-block ADMM based approach for distribution market clearing with distribution locational marginal price," *International Journal of Electrical Power & Energy Systems*, vol. 128, p. 106635, Jun. 2021.

[27] Z. Li, L. Wu, Y. Xu *et al*., "Distributed tri-layer risk-averse stochastic game approach for energy trading among multi-energy microgrids," *Applied Energy*, vol. 331, p. 120282, Feb. 2023.

[28] H. Yang, K. Zheng, W. Su *et al*., "Physically Jacobian-informed encoder-decoder ANNs for nonlinear power flow regression," *IEEE Transactions on Industry Applications*, vol. 61, no. 2, pp. 2353-2362, Mar. 2024.

[29] M. Yang, Y. Liu, L. Guo *et al*., "Hierarchical distributed chance-constrained voltage control for HV and MV DNs based on nonlinearity-adaptive data-driven method," *IEEE Transactions on Power Systems*, vol. 40, no. 1, pp. 806-819, Jan. 2024.

[30] Z. Zhang, C. Wang, Q. Wu *et al*., "Optimal dispatch for cross-regional integrated energy system with renewable energy uncertainties: a unified spatial-temporal cooperative framework," *Energy*, vol. 292, p. 130433, Apr. 2024.

[31] Y. Zhang, P. Sun, X. Ji *et al*., "Low-carbon economic dispatch of integrated energy systems considering extended carbon emission flow," *Journal of Modern Power Systems and Clean Energy*, vol. 12, no. 6, pp. 1798-1809, Nov. 2024.

[32] Y. Cheng, N. Zhang, Y. Wang *et al*., "Modeling carbon emission flow in multiple energy systems," *IEEE Transactions on Smart Grid*, vol. 10, no. 4, pp. 3562-3574, Jul. 2019.

[33] J. Ding, C. Gao, M. Song *et al*., "Optimal operation of multi-agent electricity-heat-hydrogen sharing in integrated energy system based on Nash bargaining," *International Journal of Electrical Power & Energy Systems*, vol. 148, p. 108930, Jun. 2023.

[34] Y. He, Q. Chen, J. Yang *et al*., "A multi-block ADMM based approach for distribution market clearing with distribution locational marginal price," *International Journal of Electrical Power & Energy Systems*, vol. 128, p. 106635, Jun. 2021.

[35] B. He, H. Liu, Z. Wang *et al*., "A strictly contractive Peaceman-Rachford splitting method for convex programming," *SIAM Journal on Optimization*, vol. 24, no. 3, pp. 1011-1040, Jul. 2014.

[36] A. Kargarian and Y. Fu, "System of systems-based security-constrained unit commitment incorporating active distribution grids," *IEEE Transactions on Power Systems*, vol. 29, no. 5, pp. 2489-2498, Sept. 2014.

[37] C. Wang, S. Dong, S. Xu *et al*., "Impact of power-to-gas cost characteristics on power-gas-heating integrated system scheduling," *IEEE Access*, vol. 7, pp. 17654-17662, Jan. 2019.

[38] Y. Cheng, N. Zhang, B. Zhang *et al*., "Low-carbon operation of multiple energy systems based on energy-carbon integrated prices," *IEEE Transactions on Smart Grid*, vol. 11, no. 2, pp. 1307-1318, Mar. 2020.

Yumin Zhang received the Ph.D. degree in electrical engineering from Shandong University, Jinan, China, in 2019. She is currently an Associate Professor at Shandong University of Science and Technology, Qingdao, China. Her research interests include power system operation and control, electricity market, and demand response.

Jingrui Li received the B.E. degree in electrical engineering from Shandong University of Science and Technology, Qingdao, China, in 2022. Currently, she is pursuing the M.S. degree in Shandong University of Science and Technology. Her research interests include power system operation and control.

Xingquan Ji received the Ph.D. degree in electrical engineering from Tianjin University, Tianjin, China, in 2002. He is currently a Professor at Shandong University of Science and Technology, Qingdao, China. His research interests include power system analysis and electricity market.

Zhaoyang Dong received the Ph.D. degree from the University of Sydney, Sydney, Australia, in 1999. He is a Chair Professor and Head of the Department of Electrical Engineering, City University of Hong Kong, Hong Kong, China. His previous roles include the Singapore Power Group Endowed Professor and the Co-director of Singapore Power Group-Nanyang Technological University Joint Lab, Singapore; a SHARP Professor of Energy System and the inaugral Director of University of New South Wales (NSW) Digital Grid Futures Institute, University of NSW, Sydney, Australia; the Director of ARC Research Hub for integrated energy storage systems, the Head of School of the Electrical and Information Engineering, University of Sydney; and the Ausgrid Chair Professor and the Director of Ausgrid Centre for Intelligent Electricity Networks provided Research and Development support for the Smart Grid, Smart City National Demonstration Project of Australia. He also worked with industry as a Manager for power system planning with the transmission network service provider of TAS in Australia. His research interests include power system planning and stability, smart grid, microgrid, smart city, renewable energy system, energy storage system, and energy market.

Li Yu received the Ph.D. degree from the University of New South Wales (NSW), Sydney, Australia, in 2023. She is with the Department of Electrical Engineering, City University of Hong Kong, Hong Kong, China. Her previous roles include CEO of Synco Global, Adelaide, Australia; Research Associate at Stanford University, Stanford, USA, and the University of NSW. Her research interests include power system strength assessment, electricity market, energy storage system operation, and renewable energy system.